Politecnico di Bari

Repository Istituzionale dei Prodotti della Ricerca del Politecnico di Bari

Effects of natural gas composition on performance and regulated, greenhouse gas and particulate emissions in spark-ignition engines

This is a pre-print of the following article

Original Citation:
Effects of natural gas composition on performance and regulated, greenhouse gas and particulate emissions in spark-ignition engines / Amirante, Riccardo; Distaso, Elia; Di Iorio, S.; Sementa, Paolo; Tamburrano, Paolo; Vaglieco, B. M.; Reitz, R. D.. - In: ENERGY CONVERSION AND MANAGEMENT. - ISSN 0196-8904. - 143:(2017), pp. 338-347. [10.1016/j.enconman.2017.04.016]

Availability:
This version is available at http://hdl.handle.net/11589/104810 since: 2021-03-12

Published version
DOI:10.1016/j.enconman.2017.04.016

Publisher:

Terms of use:

(Article begins on next page)

02 May 2026

Effects of Natural Gas Composition on Performance and Regulated, Greenhouse Gas and Particulate Emissions in Spark-Ignition Engines

R. Amirante[1], E. Distaso[1†], S. Di Iorio[2], P. Sementa[2], P. Tamburrano[1], B. M. Vaglieco[2] and R. D. Reitz[3]

[1] Department of Mechanics, Mathematics and Management, Polytechnic of Bari, Italy.
[2] Istituto Motori CNR, Napoli, Italy.
[3] Engine Research Center, University of Wisconsin-Madison, 1500 Engineering Drive, Madison, WI 53705, USA.

[†]Corresponding Author: Elia Distaso
Ph.D. student at Polytechnic of Bari, Italy
Visiting Scholar at Engine Research Center, University of Wisconsin-Madison, USA.
elia.distaso@poliba.it

Abstract

In vehicles fueled with compressed natural gas, a variation in the fuel composition can have non-negligible effects on their performance, as well as on their emissions. The present work aimed to provide more insight on this crucial aspect by performing experiments on a single-cylinder port-fuel injected spark-ignition engine. In particular, methane/propane mixtures were realized to isolate the effects of a variation of the main constituents in natural gas on engine performance and associated pollutant emissions. The propane volume fraction was varied from 10 to 40%. Using an experimental procedure designed and validated to obtain precise real-time mixture fractions to inject directly into the intake manifold. Indicative Mean Effective Pressure, Heat Release Rate and Mass Burned Fraction were used to evaluate the effects on engine performance. Gaseous emissions were measured as well. Particulate Mass, Number and Size Distributions were analyzed with the aim to identify possible correlations existing between fuel composition and soot emissions. Emissions samples were taken from the exhaust flow, just downstream of the valves. Opacity was measured downstream the Three-Way Catalyst. Three different engine speeds were investigated, namely 2000, 3000 and 4000 rpm stoichiometric and full load conditions were considered in all tests. The results were compared with pure methane and propane, as well as with natural gas. The results indicated that both performance and emissions were strongly influenced by the variation of the propane content. Increasing the propane fraction favored more complete combustion and increased NO_x emissions, due to the higher temperatures. In all tests, natural gas showed the highest PN values. At high speeds, adding propane increased the number of particles between 5 and 30 nm, highlighting the relevance of the ultrafine particles. Smaller differences were recorded at low speeds.

1. Introduction

Over the past several years, road transportation has seen significant advances and new alternative technologies are rapidly emerging. Energy production and storage, electric drive systems, and fuel cell technologies all seem able to find a significant place in the automotive marketplace [1–5]. However, it would be a mistake to believe that such technologies will completely replace conventional internal combustion engines in short time [6]. The need for practical mid-term solutions that can meet new fuel economy and emissions standards has pushed the development of new technologies for internal combustion engines, comprising innovative combustion techniques [7–10] as well as their control strategies [11–17].

In addition, alternative fuels are being promoted and developed to replace traditional fuels [18–22]. Natural gas represents one of the most concrete alternatives to conventional petroleum fuels (especially in the heavy-duty vehicle segment) since it produces significantly lower emissions, such as particulate matter (PM) and oxides of nitrogen (NO_x), than conventional diesel engines [8,23–25]. For these reasons, over the past eight years, 50% of the transport bus fleet in Brisbane, Australia, has been gradually converted from diesel to CNG. In New Delhi, India, one of the most polluted cities in the world, the entire transport fleet was converted to CNG in 2003 resulting in some improvement in air quality in terms of suspended particulate matter, CO, SO_2, and NO_x [26,27].

For CNG vehicles, one issue is that a variation in the fuel composition can have non-negligible effects on the combustion process [28–32]. In fact, natural gas is a mixture of various hydrocarbon molecules: the principal component is methane and its volume fraction can vary from 55.8% to 98.1%; the main heavy hydrocarbons present in natural gas are ethane, which can vary between 0.5% and 13.3% (by volume), and propane, in amounts varying between 0% and 23.7% (by volume) [33]. Diluents such as N_2 and CO_2 are also present in significant fractions. There are also trace levels of sulphur compounds, often added as odorants, and hydrocarbons larger than C_3 [30]. The components concentration change with geographical source, time of year, and treatments applied during production or transportation [34].

Previous studies have shown that changes in natural gas composition can impact emissions, as well as engine performance [28–32]. Karavalakis et al. [35] reported that natural gases with higher heating value exhibited higher fuel economy on an energy equivalent basis. Higher flame speeds and higher adiabatic flame temperatures can be obtained with larger amounts of ethane and propane in natural gas, producing more efficient combustion [30,35,36]. A reduction in Total Unburned Hydrocarbon (TUHC) emissions was seen for fuels with higher hydrocarbon contents

[29,30]. Some researchers report increases in TUHC emissions with increased ethane and propane concentration [37], although these results are not consistent with other previous studies. NO_x emission levels were clearly influenced by the fuel composition, with low Methane Number (MN) natural gases resulting in higher NO_x emissions [29–32,35]. McTaggart-Cowan et al. [30] suggested that it was due to the increased adiabatic flame temperature with a higher fraction of ethane and propane, since NO_x are generated predominantly through the strongly temperature-dependent thermal NO mechanism [38]. The authors of such work found that a 1% change in adiabatic flame temperature resulted in a 5% change in NO_x emissions. CO is another combustion by-product that is sensitive to fuel composition, but discordant results have been reported in literature [30,35].

Furthermore, current emission regulations emphasize the need to control greenhouse gas emissions from on-road sources, and consequently there is a need to control methane, as well as CO_2 emissions, from natural gas vehicles [39]. Methane is not toxic and not relevant to ozone-forming potential, but it shows a global warming potential 25 times higher than CO_2 [29]. In general, higher methane emissions were recorded for higher MN fuels [29] and this might be due to the fact that methane is less reactive than higher chain hydrocarbons, so it is more likely that higher amounts survive the combustion process [40]. Higher CO_2 emissions were recorded for natural gases having higher fraction of higher hydrocarbons [35].

McTaggart-Cowan et al. [30] found that relatively high levels of ethane and propane in natural gas can significantly increase Particulate Matter (PM) emissions. In such a study, both black carbon and volatile PM emissions were claimed to be increased by an increase in ethane and propane contents, and other studies have confirmed this trend [41]. The presence of hydrocarbons with longer chains or more complex structures can enhance PM precursor formation in the reaction zone [42,43], including C_2 species, such as the ethyl radical (C_2H_5) and acetylene (C_2H_2) [41] which are the most abundant gaseous hydrocarbon species in regions where soot is formed in laminar premixed flames [44,45].

There is a lack of information about the effect that a variation of natural gas composition can produce on Particle Number density (PN) and Size Distribution (PSD) functions. Karavalakis et al. [29] recently reported some measurements, but a clear and exhaustive understanding of the phenomenon is still needed. Therefore, substantially more work is required to understand the effects of the heavier hydrocarbons on particle formation in natural gas engines.

The present study aims to isolate the influence that hydrocarbons heavier than methane have on natural gas combustion. Ethane and propane are the other two hydrocarbons that are present in a relevant amount in natural gas. However, propane, more than ethane, has thermochemical and combustion properties that are similar to those of more complex practical fuels [46]. Therefore, it was thought that variations in its concentration would produce more appreciable effects on performance and gaseous and particulate emissions than those produced by ethane. In addition, propane is used more often than ethane in many combustion applications and laboratory studies [47]. Consequently, propane addition to pure methane was studied. Accordingly, an innovative experimental procedure was designed and validated in order to quantify real-time methane/propane fuel mixtures directly within the intake manifold. Steady-state engine performance and emissions were therefore evaluated considering different amounts of propane in methane. Experiments with pure methane, pure propane and natural gas were also performed and compared.

2. Experimental method

2.1. Apparatus

The experimental apparatus included a 4-stroke, single cylinder, port-fuel injected, SI engine, an electrical dynamometer, the methane and propane injection lines, two single-hole gas injectors, the data acquisition and control units, two Brooks SLA5800 Thermal Mass Flow Meters and Controllers, four emission measurement systems.

The engine specifications are shown in Table 1. The spark-plug was centrally located in the engine head. A modified intake manifold was employed to fit two single-hole gas injectors, allowing a simultaneous double port fuel injection. The engine was equipped with a Three-Way Catalyst (TWC) and it was water cooled. A linear lambda sensor Bosch LSU 4.9 was used to measure the air-to-fuel ratio. The engine was fueled with pure methane and propane, as well as with their mixtures and with CNG. Methane had a purity expressed in a decimal fraction equal to 3.5 and that of propane was 2.5. The natural gas composition, in terms of volume fractions of its constituents, is reported in Table 2, as provided by the suppliers.

Table 1 Engine specifications.

Name	Units	Value
Cylinder volume	cm^3	250
Bore	mm	72
Stroke	mm	60

Compression ratio	None	10.5
Number of valves	None	4
Intake Valve Opening	CAD BTDC	92
Intake valve Closure	CAD ABDC	128
Exhaust Valve Opening	CAD BBDC	128
Exhaust valve Closure	CAD ATDC	90
Max power	kW	16 at 8000 rpm
Max torque	Nm	20 at 5500 rpm

Table 2 Natural gas chemical composition.

Name	Volume Fraction
Carbon dioxide (CO_2)	1 %
Nitrogen (N_2)	2 %
Methane (CH_4)	88 %
Ethane (C_2H_6)	7 %
Propane (C_3H_8)	2 %

Gaseous and particulate emissions were measured by sampling directly from the exhausts, shortly after leaving the cylinder. CO, CO_2 were measured by means of non-dispersive infrared detectors; NO_x emissions were detected by electrochemical sensors. *A Flame Ionization Detector was used to perform a gas chromatography of the exhaust samples, allowing separation of the methane content from the total amount of UHCs measured in the exhaust*. PN concentrations and sizes were measured in the range from 5 to 560 nm by means of a TSI Engine Exhaust Particle Sizer. The exhausts were sampled and diluted with air heated at 150 °C. The dilution ratio was fixed at 1:10. A 1.5 m heated line was used for sampling the engine exhausts in order to avoid condensation of combustion water. A Volatile Particle Remover (VPR) was not used in this analysis in order to take into account all types of particles and not only the solid ones, defined by the Particle Measurement Programme [48] as the particles that can survive passing through the VPR. In addition, Opacity [%] was continuously measured by an AVL 439 Opacimeter sampling downstream the TWC.

2.2. Experimental procedure

The tests were designed to investigate the effect of natural gas composition on engine performance and emissions. In particular, the goal consisted of isolating the influence that propane has on methane combustion.

Engine performance and emissions were evaluated when the engine was fueled with pure methane and pure propane, as well as with four different mixtures, having respectively 10, 20, 30 and 40% by volume of propane in

methane. Experiments with natural gas were also performed and compared. All the tests were performed at steady state conditions. For a more extensive analysis, three different engine speeds were investigated, namely 2000, 3000 and 4000 rpm. Stoichiometric and full load conditions were kept in all tests. The list of the operating conditions is reported in Table 3. To ensure proper operation and reliable response of the exhaust gas analyzers, the engine was first warmed up and the data were recorded only after engine conditions were stabilized. Tests were repeated three times in order to provide good statistics of the measurements and each test was averaged over 300 consecutive cycles. The experimental campaign was performed at the "Istituto Motori CNR", Italy.

Table 3 Operating conditions specifications.

Speed [rpm]	Load [%]	Spark Advance [CAD ATDC]	Lambda
2000	100	-31.6	1
3000	100	-32.0	1
4000	100	-34.0	1

The in-cylinder pressure was measured by a quartz pressure transducer flush-mounted in the region between the intake and exhaust valves. It measures the in-cylinder pressure with a sensitivity of 16.2 pC/bar and a natural frequency of 130 kHz. The sensor signal was recorded by a flexible data acquisition system equipped with 8 high speed analogue inputs. In order to ensure stoichiometric conditions in all the tests, a constant monitoring and properly adjustment of the Duration Of Injections (DOIs) was realized by means of closed loop control based on the lambda value. The signals were post-processed by using the AVL IndiCom software, which allowed the calculation of combustion parameters, such as Indicating Mean Effective Pressure (IMEP), the Coefficient Of Variation (COV), the Duration of Combustion (DOC) and Heat Release Rate (HRR), as well as the crank angle at which 5, 50 and 90% of the fuel mass is burned (MBF5%, MBF50% and MBF90%).

2.2.1. Real-time fuel mixtures

An innovative experimental procedure was designed and validated to realize real-time methane/propane fuel mixtures. Two single-hole gas injectors were used to simultaneously inject two gaseous fuels within the intake manifold. An accurate control strategy, together with proper design of the injection lines, allowed precise mixture fractions and satisfactory mixing.

Figure 1 shows a schematic representation of the experimental set-up used for the mixture tests. The two gaseous fuels were supplied by pressurized bottles. Two surge tanks (numbers 3 and 4 in Figure 1) were used to absorb sudden changes in pressure due to propagating waves generated during the injection phases. This allowed stable measurements of the static injection pressures and temperatures for both gases. In addition, this ensured that the velocity of the two gases was negligible within the two tanks, thus these static measurements were representative of the total conditions upstream the two injectors. By means of two pressure regulators the injection pressure was set to 5 bar, a value that established choked flow conditions through both the injectors for all the operating conditions considered. The two fuels were injected by employing two identical single-hole injectors (numbers 5 and 6 in Figure 1).

If choked flow conditions are ensured, the average value of the mass flow rate injected, $\dot{m}_i$, is estimated by using the following expression:

$$\dot{m}_i = A_{inj} \frac{p_i^0}{\sqrt{R_i T_i^0}} \sqrt{\gamma_i} \sqrt{\left(\frac{2}{\gamma_i + 1}\right)^{\frac{\gamma_i+1}{\gamma_i-1}}} \frac{f_{inj}}{f_{inj}^{ref}}, \tag{1}$$

in which A_{inj} is the nozzle cross section area of the injector, p_i^0 and T_i^0 are the total pressure and temperature of the two gases measured in the surge tanks (numbers 3 and 4 in Figure 1), respectively, γ_i is the specific heat ratio, R_i the specific gas constant. The subscript i refers to the specific gas considered. The term f_{inj}/f_{inj}^{ref} represents the ratio between the injection frequency and its reference value at the reference case of 2000 rpm and it takes into account the fact that the injector does not work continuously, namely the mass flow rate increases proportionally with the injection frequency. Thus, a corrected mass flow rate, Γ, independent from the injection frequency, is defined as follows:

$$\Gamma = \frac{f_{inj}^{ref}}{f_{inj}} \dot{m}_i. \tag{2}$$

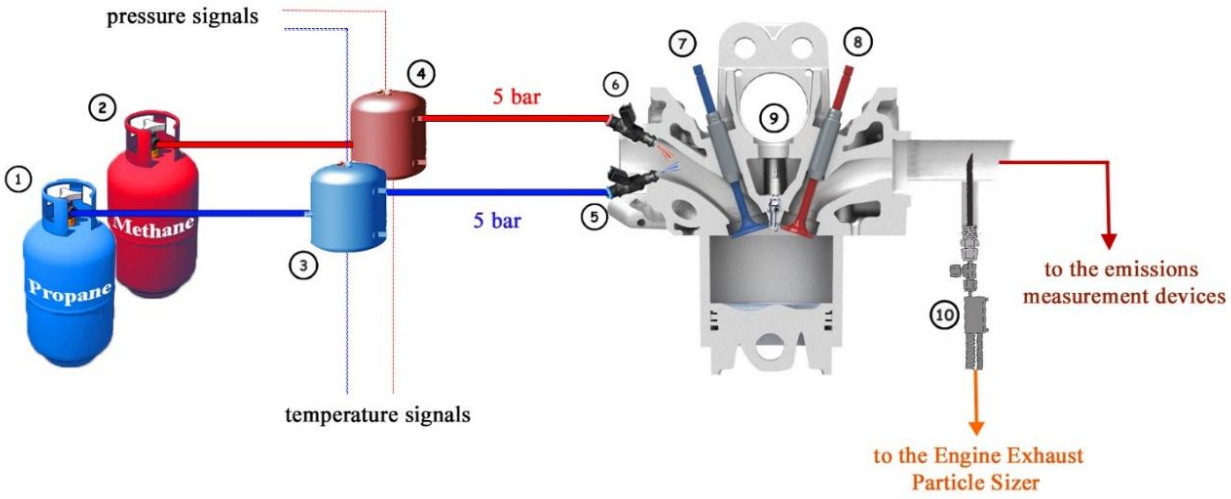

Figure 1. Experimental Set-up used for the methane/propane mixtures tests. (1) Propane bottle; (2) Methane bottle; (3) Propane surge tank; (4) Methane surge tank; (5) and (6) 1-hole gas injectors; (7) intake and (8) exhaust valves; (9) spark-plug; ; (10) particle sizer probe.

However, Equation (1) needs to be corrected in order to take into account the mechanical delay that an injector intrinsically shows. Considering that the energizing Duration Of Injection (DOI) is small for both gasses, the injection inertia cannot be neglected for obtaining accurate results. Therefore, with the aim to quantify the effect of the mechanical delay on the injected flow rate, the injector was characterized. Since preliminary tests with different gases (namely methane, propane and nitrogen) highlighted that the injector mechanical delay was fuel-independent in the range of the considered operating conditions, the experimental characterization of the injectors was carried out by using nitrogen injected at 3.5 bar.

Figure 2 (a) shows that when the DOI is short, the mass flow rate injected is significantly less than the expected value. In such a graph, the value $\Gamma = \frac{f_{inj}^{ref}}{f_{inj}} \dot{m}_{exp}$ is plotted (where $\dot{m}_{exp}$ is the experimentally measured mass flow rate). Figure 2 (b) quantifies the Deviation from the Linearity (D_L) due to the injector mechanical delay and highlights its importance. D_L was calculated by using the following expression:

$$D_L = \frac{\frac{\Gamma}{\Delta t f_{inj}^{ref}} - \Gamma_{95\%}}{\Gamma_{95\%}} 100, \quad (3)$$

where Δt is the DOI expressed in ms and $\Gamma_{95\%}$ is the value of the corrected mass flow rate measured when the DOI is equal to 95% of the engine period and it is representative of the case of a continuous injection.

Figure 2 (b) also shows that the deviation can be represented by an exponential curve having the form $-a\Delta t^{-b}$. The optimal values for the constants a and b, calculated by using a linear regression model, were found to be equal to 0.754 ms and 1.398, respectively.

Equation (1) can be therefore rewritten as:

$$\dot{m}_i = A_{inj}\frac{p_i^0}{\sqrt{R_i T_i^0}}\sqrt{\gamma_i}\sqrt{\left(\frac{2}{\gamma_i+1}\right)^{\frac{\gamma_i+1}{\gamma_i-1}}}\frac{f_{inj}}{f_{inj}^{ref}}\left(1-a\Delta t_i^{-b}\right). \quad (4)$$

The methane-to-propane mass ratio ($m_{CH_4}/m_{C_3H_8}$) can be easily calculated from the ratio between the desired mixture volume fractions ($\chi_{CH_4}/\chi_{C_3H_8}$) as:

$$\frac{m_{CH_4}}{m_{C_3H_8}} = \frac{MW_{CH_4}}{MW_{C_3H_8}}\frac{\chi_{CH_4}}{\chi_{C_3H_8}}, \quad (5)$$

where MW_{CH_4} and $MW_{C_3H_8}$ are the molecular weights of methane and propane, respectively.

Since $m_i = \dot{m}_i\Delta t_i$, Equation (5) can been rewritten as:

$$\frac{\chi_{CH_4}}{\chi_{C_3H_8}} = \frac{\zeta_{CH_4}}{\zeta_{C_3H_8}}\frac{MW_{C_3H_8}}{MW_{CH_4}}\frac{p_{CH_4}^0}{p_{C_3H_8}^0}\sqrt{\frac{T_{C_3H_8}^0}{T_{CH_4}^0}}\frac{\left(1-a\Delta t_{CH_4}^{-b}\right)\Delta t_{CH_4}}{\left(1-a\Delta t_{C_3H_8}^{-b}\right)\Delta t_{C_3H_8}}, \quad (6)$$

where $\zeta_{CH_4} = \sqrt{\frac{\gamma_{CH_4}}{R_{CH_4}}\left(\frac{2}{\gamma_{CH_4}+1}\right)^{\frac{\gamma_{CH_4}+1}{\gamma_{CH_4}-1}}}$ and $\zeta_{C_3H_8} = \sqrt{\frac{\gamma_{C_3H_8}}{R_{C_3H_8}}\left(\frac{2}{\gamma_{C_3H_8}+1}\right)^{\frac{\gamma_{C_3H_8}+1}{\gamma_{C_3H_8}-1}}}$.

Equation (6) correlates, in a direct way, the desired mixture volume fractions χ_{CH_4} and $\chi_{C_3H_8}$ with the DOIs of methane and propane $\Delta t_{CH_4}$and $\Delta t_{C_3H_8}$. A programmable electronic control unit allowed the management of the combined injection timing, according to the lambda value.

In addition, Figure 2 (a) shows that the injection frequency does not have relevant influence on the injected mass flow rate. Additional experiments demonstrated that the injection pressure does not affect the results in an appreciable way as well and this is shown in Figure 3, in which $f_{inj} = f_{inj}^{ref}$, $p_{i,ref}^0 = 3.5\ bar$ and Γ_{ref} is the corrected mass flow rate measured when $p_i^0 = p_{i,ref}^0$. Different DOIs were considered for a more exhaustive analysis.

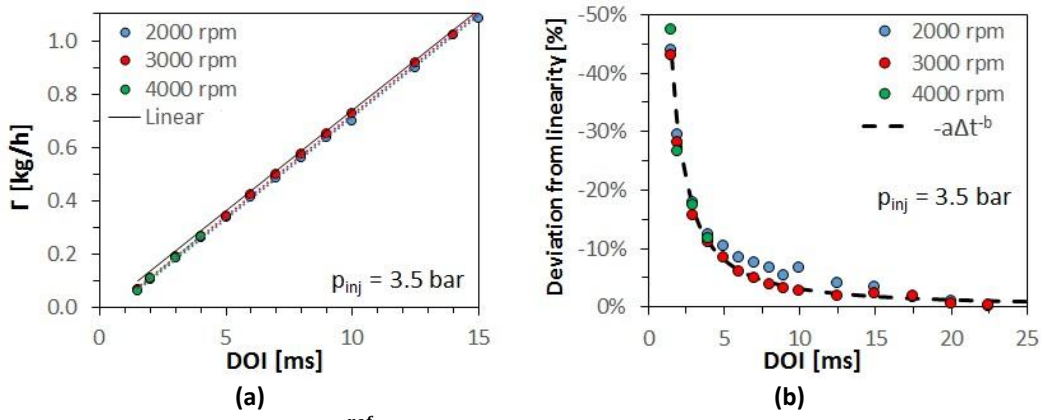

Figure 2. Measured mass flow rate $\boldsymbol{\Gamma = \frac{f_{inj}^{ref}}{f_{inj}} \dot{m}_{exp}}$ (a). Deviation from linearity due to injector mechanical delay (b).

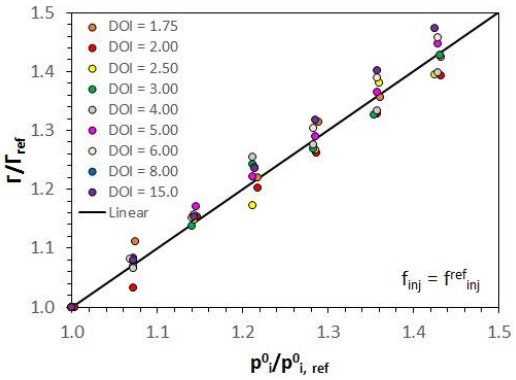

Figure 3. Linearity of the mass flow rate $\boldsymbol{\Gamma}$ from the injection pressure $\boldsymbol{p_i^0}$. In the graph $\boldsymbol{p_{i,ref}^0 = 3.5\ bar}$ and $\boldsymbol{\Gamma_{ref}}$ is the mass flow rate measured when $\boldsymbol{p_i^0 = p_{i,ref}^0}$. Experiments carried out with $\boldsymbol{f_{inj} = f_{inj}^{ref}}$.

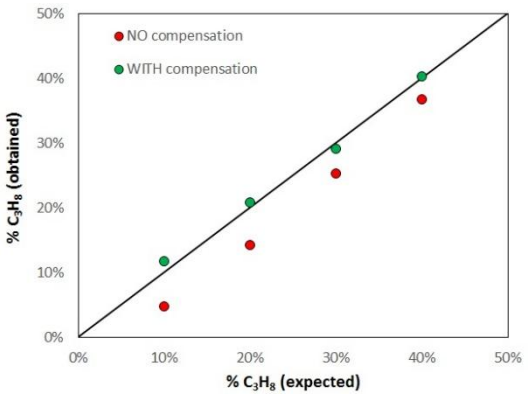

Figure 4. Expected vs measured propane fraction. Red marks refer to $\boldsymbol{\Delta t_{CH_4}}$ and $\boldsymbol{\Delta t_{C_3H_8}}$ calculated by using Equation (1), while green marks refer to $\boldsymbol{\Delta t_{CH_4}}$ and $\boldsymbol{\Delta t_{C_3H_8}}$ calculated by using Equation (4).

2.2.2. Mixing procedure validation

The procedure was validated by analyzing the obtained mixtures with the flame ionization detector during motoring conditions. The sample was properly diluted to meet the instrument working range. In this way, it was possible to check if the composition of the obtained fuel blends corresponded to that which was expected. The results are shown in Figure 4. The use of Equation (2) (green symbols) gave more than satisfactory results. It was confirmed that the injector's mechanical delay needs to be considered in calculations by comparing the results obtained with Equation (1) (red symbols in Figure 4). In the latter case, the injected mass of propane was overestimated more than that of methane, giving a lower fraction of propane in the resulting mixture. This because the DOI for propane was shorter than that for methane and the effects of the injector inertia were stronger (see Figure 2 (b)).

Finally, to ensure proper mixing of the two gasses within the intake manifold, it was chosen to inject twice per cycle. This strategy ensured the longest time possible for the mixing process, and turbulence within the intake ducts helped the process. The measurements depicted in Figure 4 never showed a deviation of the recorded value larger than 0.5%, giving confidence that the mixing process was satisfactory. In addition, performance and emissions measurements (reported in next sections) did not show any appreciable fluctuations attributable to possible not-perfect mixing.

3. Results and discussion

In the next sections the effect of propane addition to methane on engine performance is first described. Then, the influence on regulated and greenhouse gas emissions is illustrated. For the various methane/propane mixtures the nomenclature P10, P20, P30 and P40 is used in the next section, where the number denotes the propane volume fraction in the mixture.

3.1. Engine performance

Varying the fuel composition had a significant influence on the combustion event and therefore on the engine performance. These influences are summarized in Figure 5 and in Figure 6, where the in-cylinder pressure traces, and HRR, IMEP, COV and DOC are represented for each of the engine speeds considered.

Figure 6 (a) and (b) show that for all mixtures and conditions, the effect of propane addition was to increase the IMEP and, at the same time, to reduce the COV. In other words, propane presents a more stable and efficient combustion process than methane and therefore, even when small amounts of it are added to methane, it is possible to appreciate beneficial effects on engine performance. These results are easily explainable by comparing the physical and chemical property of the tested gas. Propane has a faster burning speed than methane [47,49,50], thus as the mixture was ignited the in-cylinder pressure increased faster when propane was added to methane for all engine speeds, as shown in Figure 5. The larger the propane fraction in methane, the higher was the obtained pressure-peak, as well as the higher was the HHR-peak, which means that a larger amount of energy was released in the initial combustion phases. This is also appreciable from the progressively lower MBF5% values obtained adding propane. This behaviour can be explained by considering that, in addition to a faster burning velocity, propane also features a chemical structure that allows it to be ignited easier. For alkane fuels heavier than methane, the initiation reactions occur mainly through the breaking of a C-C bond since the C-H bond has a much higher bond dissociation energy. The longer the chain, the easier is its breaking into smaller intermediate hydrocarbons and chain propagating radicals [51].

The fact that propane addition speeds up the combustion process is also visible in Figure 6 (c) when the cases of 3000 and 4000 rpm are considered. The graphs report the values of the DOC, calculated as the difference between the CADs corresponding to MBF90% and MBF5%.

Contrariwise, when the engine run at 2000 rpm the DOC increased slightly with gradual propane addition. This means that the ending phase of the combustion process was not as fast as the initial one for propane mixtures, as can be inferred from the HRR traces at 2000 rpm in Figure 5. This can be attributed to the fact that, once the flame reaches the cylinder walls, the combustion is completed in the absence of a propagating flame and depends on only chemistry. In the last phase of combustion most likely the conversion reactions from CO to CO_2 are taking place, which are commonly considered the slowest part of the oxidation process. In the case of propane and its mixtures the flame reaches the cylinder walls earlier than methane and therefore the ending part of the combustion assumes more relevant importance. At higher speeds, the final oxidation process is enhanced by the increased turbulence.

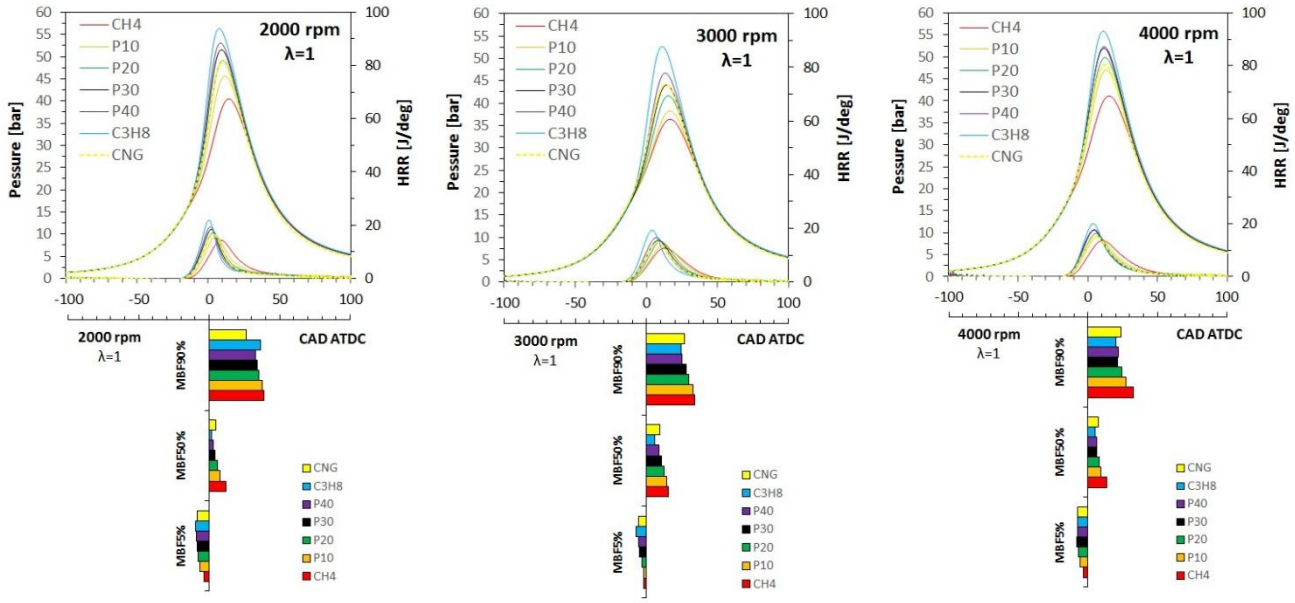

274 **Figure 5.** In-cylinder pressure, HRR, MBF5%, MBF50% and MBF90% for the three different engine speeds investigated.

275

276

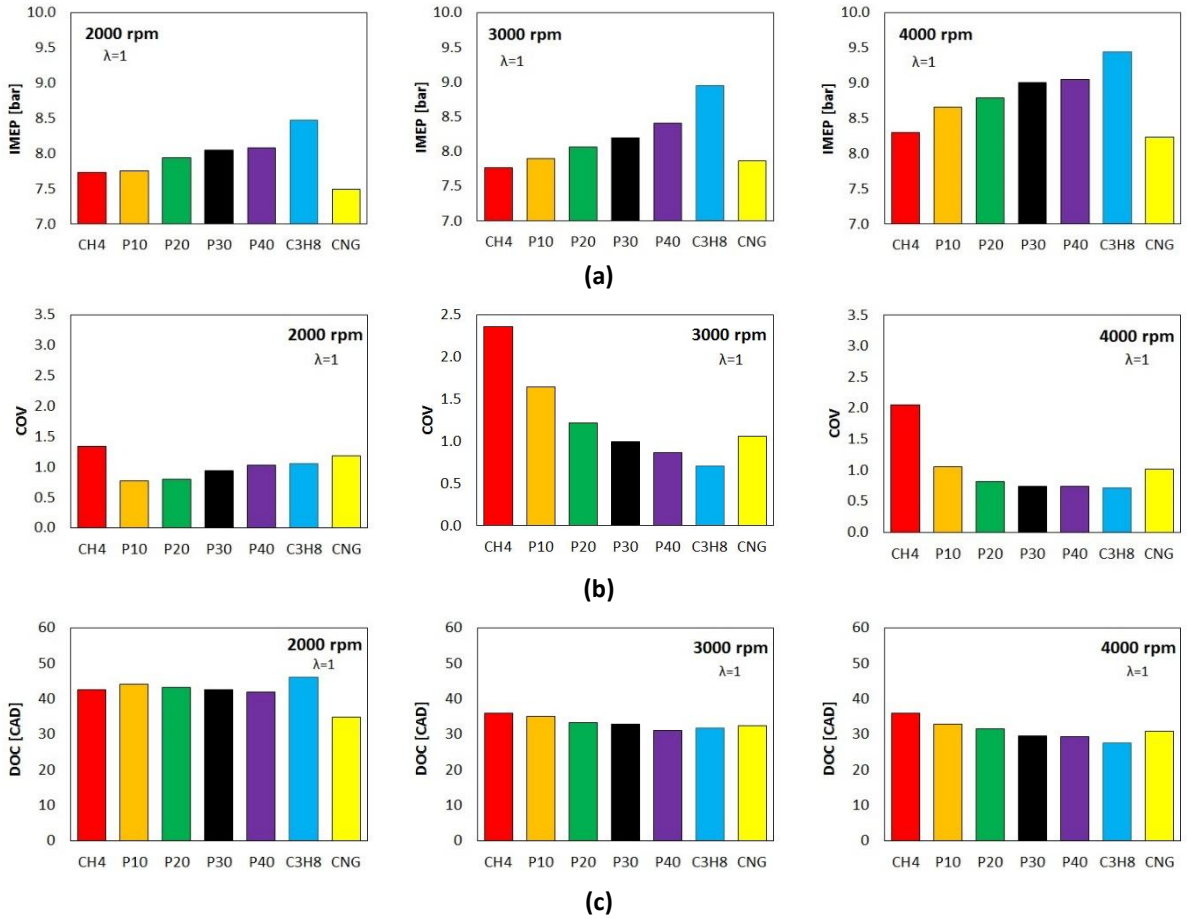

277 **Figure 6.** IMEP (a) COV (b) and DOC (c) for the three different engine speeds investigated.

278

Natural gas recorded in-cylinder pressure and calculated HRR traces, as well as MBF5% values (Figure 5), were in-between those of the two pure compounds and, in particular, they were close to the case with a propane fraction in methane equal to 20% (the natural gas contained appreciable ethane, which has a faster flame speed than propane [47,49,50]). However, the presence of diluents, such as N_2 and CO_2 (Table 2), explains why the recorded values of IMEP (Figure 6 (a)) were comparable to or lower than those obtained when the engine was fueled with pure methane [52]. The presence of the small fraction of heavier hydrocarbons ensured, for the aforementioned reasons, lower values of COV (Figure 6 (b)) and DOC (Figure 6 (c)) than for pure methane.

3.2 Regulated and greenhouse emissions

The values recorded for regulated and greenhouse emissions are reported and the error bars on the graphs represent the standard deviation of the measurements. The UHC emissions are reported in Figure 7 for the three different engine speeds investigated. For methane, the great part of UHC emissions was predominantly CH_4 emissions (unburned methane). Analogous behavior was recorded for natural gas, since methane is its main constituted. However, the TUHC level was higher than pure methane and this can be attributed to the presence of heavier hydrocarbons within the natural gas. The recorded value of CH_4 emissions decreased as the propane content in methane/propane mixtures was increased, while, even though the non-methane part increased, the TUHCs decreased when propane was added. The fastest combustion process, together with the higher temperature reached with the presence of propane favors a more complete combustion, explaining the obtained results, that are in agreement with previous studies [29,30,35,36].

The more complete conversion of fuel into CO and CO_2 can also explain their gradually increased values with an increase of propane concentration, as shown in Figure 8. This agrees with the interpretation that the UHC emissions are primarily unreacted fuel, while the CO is a by-product of partial combustion [30]. When natural gas is burned the conversion rate into CO is increased by the heavier hydrocarbons, while the presence of diluents slows down the final conversion process of CO into CO_2.

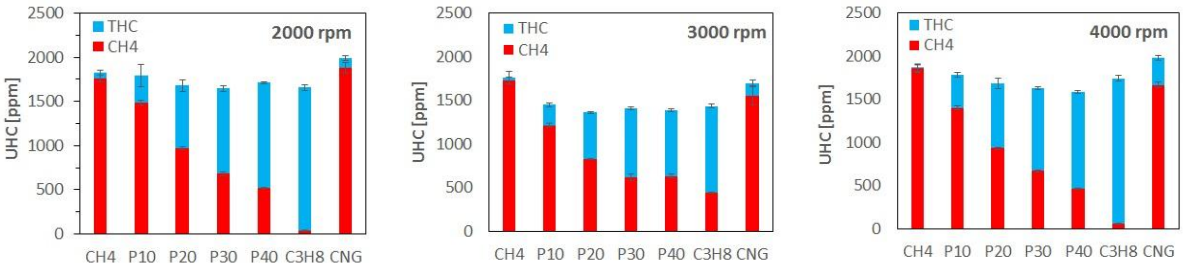

Figure 7. TUHC (blue bars) and CH_4 (red bars) emissions for the three different engine speeds investigated.

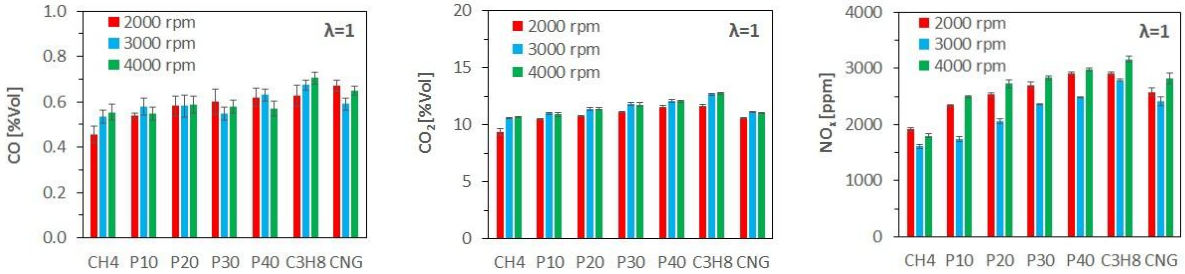

Figure 8. CO, CO_2 and NO_x emissions for the three different engine speeds investigated.

Figure 8 also shows that the NO_x emissions tend to be one of the most sensitive to combustion conditions. When the engine is fueled with propane, higher temperatures are reached within the combustion chamber, due to its higher adiabatic flame temperature than methane. Therefore, higher levels of NO_x are expected. Also, the presence of propane and ethane, as well as of heavier hydrocarbons in the natural gas promotes the formation of reactive radicals, resulting in an increased formation of prompt NO_x [29]. This explains both the highest value recorded for pure propane and the intermediate values recorded for natural gas. The present results agree with previous studies that have reported higher NO_x emissions with low MN fuels [29–32,35].

The case of 3000 rpm exhibited the lowest NO_x levels in comparison to the other two engine speeds for all considered fuels. It must be noted that this case showed the highest levels of COV (Figure 6 (a)), symptomatic of higher combustion instability compared to the other cases, probably due to particular turbulence conditions that characterize the test engine. As a consequence, the recorded in-cylinder pressure peaks were lower (Figure 5) and therefore lower temperature were reached, explaining the lower NO_x levels.

3.3. Particulate emissions

Measured PSD functions are depicted in Figure 9. At 2000 rpm, the difference between the methane/propane mixtures were small, although with 40% of propane in methane and more clearly with pure propane, particles with size between 15 and 30 nm started to become predominant and the distribution assumed a shape very similar to that recorded for natural gas. There are evidences in the literature that correlate an increase in soot emissions with an increase in ethane and propane content in natural gas [30,41], and this behaviour is commonly attributed to enhanced soot precursor formation in the reaction zone, such as C_2H_2 and C_2H_5, which are important intermediates in the chemical reaction path generated in the combustion of heavier hydrocarbons. This explains, at least partially, why natural gas showed the highest values of particles emitted by the engine, which resulted in the highest total PN levels shown in Figure 10 (a). An additional contribution is due to the presence of diluents in natural gas that are responsible of a less stable and efficient combustion (as previously discussed). The result is an enhanced soot precursor formation attributable to the presence of ethane and propane, followed by a reduced oxidation capability due to the presence of CO_2 and N_2 in natural gas [52].

When the engine speed is lower, more time is available during the expansion stroke for oxidation, which is also enhanced by the higher temperatures reached with the presence of propane. Thus, if a larger amount of soot was generated with slightly increased amounts of propane in methane, it was also oxidized faster, resulting in a final level that was comparable to that detected for pure methane.

Increasing the engine speed resulted in a general increase in the number of particles emitted. At 4000 rpm, increasing the propane content produced an increase in the number of particles below 30 nm. This is a relevant result considering that in Euro VI heavy duty emission regulations, only non-volatile particles over 23 nm are taken into account [48].

What appears noticeable is the fact that mixtures with a smaller amount of propane generated a lower number of particles near the distribution peak, namely 50 nm, resulting in a lower total PN value (Figure 10 (a)). This might be due to the fact that small amounts of propane can increase the mixture's oxidation ability more than its soot tendency. However, the number of particles with the finest dimension were always increased with an increase of propane fraction.

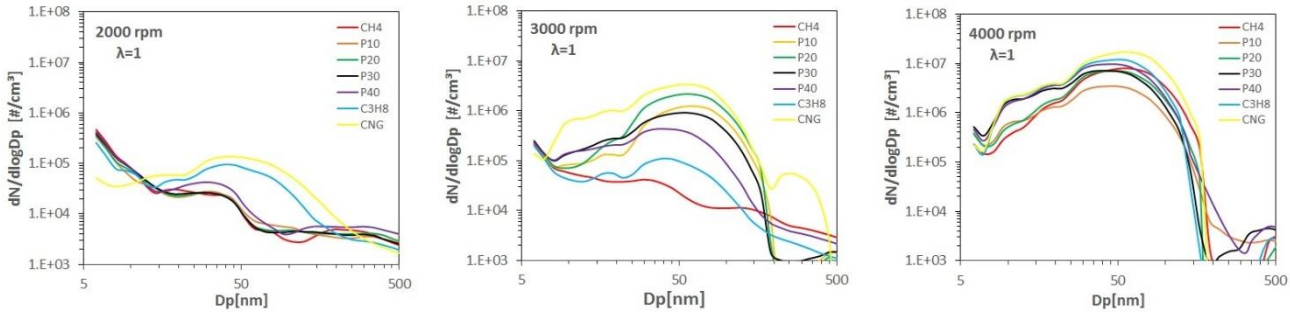

352 **Figure 9.** PSD functions for the three different engine speeds investigated.

353

354

355

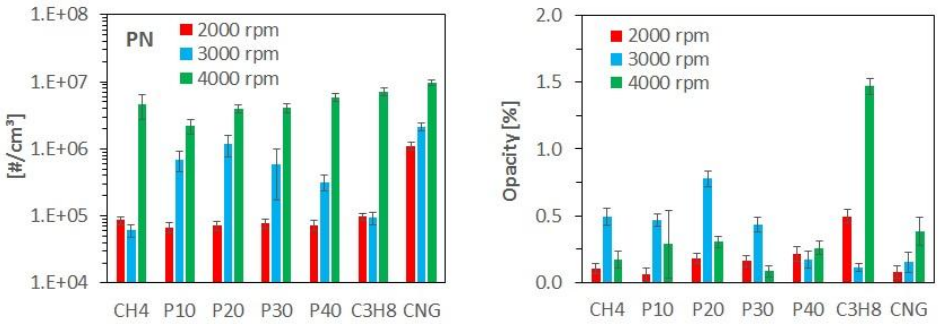

356 **Figure 10.** PN (a) and PM (b) for the three different engine speeds investigated.

357

358 In the central graph of Figure 9 is plotted the intermediate case of 3000 rpm. It shows a different behavior from both
359 the two previous cases, and this could be mainly attributable to the abovementioned turbulence conditions that
360 characterize this engine speed. This highlights the sensitivity of the soot formation process to the thermo-physical
361 combustion conditions. It was confirmed that the highest number of particles were emitted by the natural gas
362 combustion and the lowest by that of methane. A gradual increase of propane fraction in methane first produced an
363 increase in PN and then, for larger fractions, a decrease, as shown in Figure 10 (a). The particles with size of about 50
364 nm showed the greatest sensitivity to these conditions (Figure 9).

365 The trends recorded by the spectrometer were confirmed by opacity measurements of soot mass, and the results are
366 reported in Figure 10 (b). However, some differences can be highlighted, e.g., the recorded values for natural gas were
367 lower than propane and the highest opacity values were recorded at 3000 rpm. These discrepancies could be due to
368 the following reasons: first, the opacity samples were collected downstream the TWC to avoid interference between

369 the various instrument probes. Second, only the largest particles can be efficiently measured by the opacimeter
370 device. In addition, the recorded values were close to the lower detection limit of the instrument.

371

372 4. Conclusions

373 The present study reports the influence of natural gas composition on the performance and emissions of a single-
374 cylinder port-fuel injected SI engine. The work focuses on the effects generated by a modification in the heavier
375 hydrocarbons content and, in particular, propane addition to pure methane. To pursuit this aim, an innovative
376 experimental procedure was designed and validated to realize real-time methane/propane fuel mixtures directly
377 within the intake manifold. The propane volume fraction was varied from 10 to 40%. In addition, experiments with
378 pure methane, pure propane and natural gas were also performed and compared. Mean Effective Pressure, Heat
379 Release Rate and Mass Burned Fraction were used to evaluate the effects on engine performance. Gaseous emissions,
380 particulate mass, number and size distributions were analyzed with the aim to identify existing correlations between
381 fuel composition and pollutant emissions.

382 For all mixtures and conditions, the effect of propane addition was to increase the IMEP value and, at the same time,
383 to reduce the COV, resulting in more stable and efficient combustion than pure methane. For the natural gas case, the
384 presence of heavier hydrocarbons ensured lower values of COV and DOC than pure methane.

385 CH_4 emissions (unburned methane) decreased as the propane content in methane/propane mixtures was increased,
386 while, even though the non-methane part increased, the TUHCs (total) decreased when propane was added. The
387 faster combustion process, together with higher temperatures obtained with the presence of propane favor more
388 complete combustion, which can also explain the increased values of CO_2, as well as the higher levels of NO_x. For
389 natural gas, the conversion rate into CO is increased by the heavier hydrocarbons, while the presence of diluents
390 results in a slower conversion process of CO into CO_2. The enhanced formation of reactive radicals and the due to the
391 heavier hydrocarbons explains the higher NO_x emissions for natural gas in comparison to pure methane.

392 In all tests, natural gas showed the highest PN values. At 4000 rpm, increasing the propane content produced an
393 increase in the number of particles between 5 and 30 nm, highlighting the relevance of the ultrafine particles,
394 especially at the highest speeds. Larger differences in PSDs were detected at intermediate speeds and this was

attributed to the engine turbulence at this condition. This highlights the sensitivity of the soot formation process to the thermo-physical conditions occurring within the combustion chamber.

In the future, the need for even cleaner and better performing engines will need to increase performance and at same time reduce pollutant emissions of engine fueled with compressed natural gas. Controlling the composition of this gas, with addition of hydrocarbons and diluents content, could represent an interesting solution. Therefore, further investigations are needed in which different conditions in terms of equivalence ratio, and energy content of the fuel are of interest. The effect of varying natural gas additives should be considered as well. In addition, it is crucial to perform studies in which the fuel composition contribution to particle emissions is separated from that of the lubricant oil, which is known to be a major source of PM in natural gas engines and can affect the results, since lubricating oil-originated hydrocarbons and sulfur compounds can magnify the existing particles in the dilution and cooling process.

Acknowledgments

The authors are grateful to Carlo Rossi, Bruno Sgammato and Davide Pettinicchio, for their invaluable technical support during the entire experimental campaign.

Nomenclature

$\dot{m}_i$	Mass flow rate
$\dot{m}_{exp}$	Measured mass flow rate
m_{CH_4}	Methane injected mass
$m_{C_3H_8}$	Propane injected mass
χ_{CH_4}	Methane volume fraction
$\chi_{C_3H_8}$	Propane volume fraction
MW_{CH_4}	Methane molecular weight
$MW_{C_3H_8}$	Propane molecular weight
ζ_{CH_4}	Constant in Equation (6) relative to methane
$\zeta_{C_3H_8}$	Constant in Equation (6) relative to propane
Γ	Corrected mass flow rate with respect to the injection frequency
$\Gamma_{95\%}$	Corrected mass flow rate measured when $p_i^0 = p_{i,ref}^0$
Γ_{ref}	Value of the corrected mass flow rate measured when the DOI is equal to 95%

D_L	Deviation from the Linearity
A_{inj}	Nozzle cross section area of the injector
p_i^0	Total injection pressure
$p_{i,ref}^0$	Reference total injection pressure, equal to 3.5 bar
T_i^0	Total injection temperature
R_i	Specific heat ratio
γ_i	Specific heat ratio
f_{inj}	Injection frequency, equal to 33.33 injection per cycle
f_{inj}^{ref}	Reference injection frequency
Δt_i	Duration of injection
Γ	Corrected mass flow rate
a, b	Correction constants in Equations (4) and (6)
i	Refers to either methane or propane

Definitions/Abbreviations

ABDC	After Bottom Dead Center
ATDC	After Top Dead Center
BBDC	Before Bottom Dead Center
BTDC	Before Top Dead Center
CNG	Compressed natural gas
COV	Coefficient Of Variation
DOC	Duration of Combustion
DOC	Duration of Combustion
DOI	Duration Of Injection
HHR	Heat release ratio
HRR	Heat Release Rate
IMEP	Indicating Mean Effective Pressure
MBF	Mass Burned Fraction
MN	Methane Number
NO_x	Oxides of Nitrogen
PM	Particulate matter
PN	Particle number
PSDs	particle size distributions
TUHCs	Total Unburned Hydrocarbons
TWC	Three-way catalyst
UHCs	Unburned Hydrocarbons
VPR	Volatile Particle Remover

References

[1] Gao D, Jin Z, Zhang J, Li J, Ouyang M. Development and performance analysis of a hybrid fuel cell/battery bus with an axle integrated electric motor drive system. Int J Hydrogen Energy 2016;41:1161–9.

[2] Alaswad A, Baroutaji A, Olabi AG. Application of Fuel Cell Technologies in the Transport Sector. Current Challenges and Developments. State Art Energy Dev 2015;11:251.

[3] Amirante R, Cassone E, Distaso E, Tamburrano P. Overview on recent developments in energy storage: Mechanical, electrochemical and hydrogen technologies. Energy Convers Manag 2017;132:372–87.

[4] Amirante R, Tamburrano P. Novel, cost-effective configurations of combined power plants for small-scale cogeneration from biomass: Feasibility study and performance optimization. Energy Convers Manag 2015;97:111–20.

[5] Catalano LA, De Bellis F, Amirante R, Rignanese M. An Immersed Particle Heat Exchanger for Externally Fired and Heat Recovery Gas Turbines. J Eng Gas Turbines Power 2011;133:32301.

[6] Lave LB, Maclean HL. An environmental-economic evaluation of hybrid electric vehicles : Toyota's Prius vs its conventional internal combustion engine Corolla. Transp Res Part D Transp Environ 2002;7:155–62.

[7] Hofmann P, Hofherr T, Hoffmann G, Preuhs J-F. Potential of CNG Direct Injection for Downsizing Engines. MTZ Worldw 2016;77:28–35.

[8] Walker NR, Wissink ML, DelVescovo DA, Reitz RD. Natural Gas for High Load Dual-Fuel Reactivity Controlled Compression Ignition in Heavy-Duty Engines. J Energy Resour Technol 2015;137:42202.

[9] Benajes J, Garcia A, Monsalve-Serrano J, Boronat V. Achieving clean and efficient engine operation up to full load by combining optimized RCCI and dual-fuel diesel-gasoline combustion strategies. Energy Convers Manag 2017;136:142–51.

[10] Kalsi SS, Subramanian KA. Experimental investigations of effects of EGR on performance and emissions characteristics of CNG fueled reactivity controlled compression ignition (RCCI) engine. Energy Convers Manag 2016;130:91–105.

[11] Fathi M, Jahanian O, Shahbakhti M. Modeling and controller design architecture for cycle-by-cycle combustion control of homogeneous charge compression ignition (HCCI) engines--A comprehensive review. Energy Convers Manag 2017;139:1–19.

[12] Wermuth N, Najt PM, Yun H. Control strategy for transitions between homogeneous-charge compression-ignition and spark-ignition combustion modes. US Patent 8.955.492, 2015.

[13] Amirante R, Casavola C, Distaso E, Tamburrano P, Bari P. Towards the Development of the In-Cylinder Pressure Measurement Based on the Strain Gauge Technique for Internal Combustion Engines Operating Principles of the Proposed Strain. 2015-24-2419 SAE Tech Pap 2015.

[14] Benajes J, Molina S, Garcia A, Monsalve-Serrano J, Durrett R. Performance and engine-out emissions evaluation of the double injection strategy applied to the gasoline partially premixed compression ignition spark assisted combustion concept. Appl Energy 2014;134:90–101.

[15] Finesso R, Spessa E, Yang Y. Fast estimation of combustion metrics in DI diesel engines for control-oriented applications. Energy Convers Manag 2016;112:254–73.

[16] Yousefzadeh A, Jahanian O. Using detailed chemical kinetics 3D-CFD model to investigate combustion phase of a CNG-HCCI engine according to control strategy requirements. Energy Convers Manag 2017;133:524–34.

[17] Amirante R, Coratella C, Distaso E, Rossini G, Tamburrano P. An Optical Device for Measuring the Injectors Opening in Common Rail Systems. Int J Automot Technol 2017:In press.

[18] Khalilarya S, Nemati A, others. A numerical investigation on the influence of EGR in a supercharged SI engine fueled with gasoline and alternative fuels. Energy Convers Manag 2014;83:260–9.

[19] Zhang B, Ji C, Wang S. Investigation on the lean combustion performance of a hydrogen-enriched n-butanol engine. Energy Convers Manag 2017;136:36–43.

[20] Zeng K, Huang Z, Liu B, Liu L, Jiang D, Ren Y, et al. Combustion characteristics of a direct-injection natural gas engine under various fuel injection timings. Appl Therm Eng 2006;26:806–13.

[21] Salahi MM, Esfahanian V, Gharehghani A, Mirsalim M. Investigating the reactivity controlled compression ignition (RCCI) combustion strategy in a natural gas/diesel fueled engine with a pre-chamber. Energy Convers Manag 2017;132:40–53.

[22] Rinaldini CA, Allesina G, Pedrazzi S, Mattarelli E, Savioli T, Morselli N, et al. Experimental investigation on a Common Rail Diesel engine partially fuelled by syngas. Energy Convers Manag 2017;138:526–37.

[23] Cho HM, He BQ. Spark ignition natural gas engines-A review. Energy Convers Manag 2007;48:608–18.

[24] Korakianitis T, Namasivayam AM, Crookes RJ. Natural-gas fueled spark-ignition (SI) and compression-ignition (CI) engine performance and emissions. Prog Energy Combust Sci 2011;37:89–112.

[25] Hallquist ÅM, Jerksjö M, Fallgren H, Westerlund J, Sjödin Å. Particle and gaseous emissions from individual diesel and CNG buses. Atmos Chem Phys 2013;13:5337–50.

[26] Goyal P, Sidhartha. Present scenario of air quality in Delhi: A case study of CNG implementation. Atmos Environ 2003;37:5423–31.

[27] Jayaratne ER, Meyer NK, Ristovski ZD, Morawska L, Miljevic B. Critical analysis of high particle number emissions from accelerating compressed natural gas buses. Environ Sci Technol 2010;44:3724–31.

[28] Aesoy V, Valland H. The Influence of Natural Gas Composition on Ignition in a Direct Injection Gas Engine Using Hot Surface Assisted Compression Ignition. 961934 SAE Tech Pap 1996.

[29] Karavalakis G, Hajbabaei M, Jiang Y, Yang J, Johnson KC, Cocker DR, et al. Regulated, greenhouse gas, and particulate emissions from lean-burn and stoichiometric natural gas heavy-duty vehicles on different fuel compositions. Fuel 2016;175:146–56.

[30] Mctaggart-cowan GP, Rogak SN, Munshi SR, Hill PG, Bushe WK. The influence of fuel composition on a heavy-duty , natural-gas direct-injection engine. Fuel 2010;89:752–9.

[31] Feist MD, Landau M, Harte E. The Effect of Fuel Composition on Performance and Emissions of a Variety of Natural Gas Engines. SAE Int J Fuels Lubr 2010;3:100–17.

[32] Hajbabaei M, Karavalakis G, Johnson KC, Lee L, Durbin TD. Impact of natural gas fuel composition on criteria, toxic, and particle emissions from transit buses equipped with lean burn and stoichiometric engines. Energy 2013;62:425–34.

[33] Liss WE, Thrasher WH, Steinmetz GF, Chowdiah P, Attari A. Variability of natural gas composition in select major metropolitan areas of the United States. Pap No GRI-92/0123 1992.

[34] Richards GA, McMillian MM, Gemmen RS, Rogers WA, Cully SR. Issues for low-emission, fuel-flexible power systems. Prog Energy Combust Sci 2001;27:141–69.

[35] Karavalakis G, Hajbabaei M, Durbin TD, Johnson KC, Zheng Z, Miller WJ. The effect of natural gas composition on the regulated emissions, gaseous toxic pollutants, and ultrafine particle number emissions from a refuse hauler vehicle. Energy 2013;50:280–91.

505 [36] Yossefi D, Belmont MR, Ashcroft SJ, Maskell SJ. A comparison of the relative effects of fuel
506 composition and ignition energy on the early stages of combustion in a natural gas spark ignition
507 engine using simulation. Proc Inst Mech Eng Part D-Journal Automob Eng 2000;214:383–93.

508 [37] Min B, Bang K, Kim H, Chung J. Effects of gas composition on the performance and hydrocarbon
509 emissions for CNG engines. 981918 SAE Tech Pap 1998.

510 [38] Miller JA, Bowman CT. Mechanism and modeling of nitrogen chemistry in combustion. Prog Energy
511 Combust Sci 1989;15:287–338.

512 [39] Stanton DW. Systematic development of highly efficient and clean engines to meet future
513 commercial vehicle greenhouse gas regulations. SAE Int J Engines 2013;6:1395–480.

514 [40] Burcat A, Scheller K, Lifshitz A. Shock-tube investigation of comparative ignition delay times for C1-
515 C5 alkanes. Combust Flame 1971;16:29–33.

516 [41] Huang J, Bushe WK. Experimental and kinetic study of autoignition in methane / ethane / air and
517 methane / propane / air mixtures under engine-relevant conditions. Combust Flame 2006;144:74–
518 88.

519 [42] El-Sherif AS. Effects of natural gas composition on the nitrogen oxide, flame structure and burning
520 velocity under laminar premixed flame conditions. Fuel 1998;77:1539–47.

521 [43] Caillol C, Delorme T, Denis P, Berardi G. A Combustion Model for Analyzing the Effects of Natural Gas
522 Composition on the Operation of a Spark Ignition Engine. SAE Tech Pap Ser 2002:1–10.

523 [44] Amirante R, Distaso E, Tamburrano P, Bari P, Reitz RD. Measured and Predicted Soot Particle
524 Emissions from Natural Gas Engines. 2015-24-2518 SAE Tech Pap 2015.

525 [45] Jiao Q, Reitz RD. Modeling soot emissions from wall films in a direct-injection spark-ignition engine.
526 Int J Engine Res 2014;16:994–1013.

527 [46] Gülder ÖL. Correlations of laminar combustion data for alternative SI engine fuels. 841000 SAE Tech
528 Pap 1984.

529 [47] Bosschaart KJ, De Goey LPH. The laminar burning velocity of flames propagating in mixtures of
530 hydrocarbons and air measured with the heat flux method. Combust Flame 2004;136:261–9.

531 [48] Giechaskiel B, Chirico R, Decarlo PF, Clairotte M, Adam T, Martini G, et al. Science of the Total
532 Environment Evaluation of the particle measurement programme (PMP) protocol to remove the
533 vehicles' exhaust aerosol volatile phase. Sci Total Environ 2010;408:5106–16.

534 [49] Ranzi E, Frassoldati A, Grana R, Cuoci A, Faravelli T, Kelley AP, et al. Hierarchical and comparative
535 kinetic modeling of laminar flame speeds of hydrocarbon and oxygenated fuels. Prog Energy
536 Combust Sci 2012;38:468–501.

537 [50] Dirrenberger P, Gall L, Bounaceur R, Herbinet O, Glaude P, Konnov A, et al. Measurements of
538 Laminar Flame Velocity for Components of Natural Gas. Energy & Fuels 2011;25:3875–84.

539 [51] Khalil EB, Karim GA. A Kinetic Investigation of the Role of Changes in the Composition of Natural Gas
540 in Engine. Trans Soc Mech Eng J Eng Gas Turbines Power 2002;124:404–11.

541 [52] Wang Z, Zuo H, Liu Z, Li W, Dou H. Impact of N 2 dilution on combustion and emissions in a spark
542 ignition CNG engine. Energy Convers Manag 2014;85:354–60.

543